

# TECHNICAL RESEARCH REPORT

## Influence of Gas Composition on Wafer Temperature Control in a Tungsten Chemical Vapor Deposition Reactor

*by H.-Y. Chang, R.A. Adomaitis, J.N. Kidder, Jr.,  
G.W. Rubloff*

**T.R. 2000-9**



*ISR develops, applies and teaches advanced methodologies of design and analysis to solve complex, hierarchical, heterogeneous and dynamic problems of engineering technology and systems for industry and government.*

*ISR is a permanent institute of the University of Maryland, within the Glenn L. Martin Institute of Technology/A. James Clark School of Engineering. It is a National Science Foundation Engineering Research Center.*

**Web site <http://www.isr.umd.edu>**

# Influence of Gas Composition on Wafer Temperature Control in a Tungsten Chemical Vapor Deposition Reactor

**Hsiao-Yung Chang and Raymond A. Adomaitis\***

*Department of Chemical Engineering and Institute for Systems Research*

*University of Maryland, College Park MD 20742*

**John N. Kidder, Jr. and Gary W. Rubloff**

*Department of Material Science and Engineering and Institute for Systems Research*

*University of Maryland, College Park MD 20742*

March 15, 2000

## **Abstract**

Experimental measurements of wafer temperature in a single-wafer, lamp-heated CVD system were used to study the wafer temperature response to gas composition. A physically based simulation procedure for the process gas and wafer temperature was developed in which a subset of parameter values were estimated using a nonlinear, iterative parameter identification method, producing a validated model with true predictive capabilities. With process heating lamp power held constant, wafer temperature variations of up to 160K were observed by varying feed gas H<sub>2</sub>/N<sub>2</sub> ratio. Heat transfer

---

\*To whom all correspondence should be addressed. E-mail: adomaiti@isr.umd.edu

between the wafer and susceptor was studied by shifting the instrumented wafer off the susceptor axis, exposing a portion of the wafer backside to the chamber floor. Model predictions and experimental observations both demonstrated that the gas velocity field had little influence on the observed wafer and predicted gas temperatures.

**Keywords** Chemical vapor deposition, Gas thermal conduction, Heat transfer modeling, Method of weighted residuals, Parameter estimation.

## I. Introduction

Physically based process modeling and simulation methods have been gradually adopted as a design tool in the development of semiconductor manufacturing equipment. The value of process modeling is underscored by its broad acceptance [1, 2, 3, 4, 5, 6] in the control systems designed to meet the more stringent requirements imposed by continually shrinking device sizes. The flexibility of simulation tools can be exploited to test the conceptual feasibility of new design ideas in early stages of equipment development, reduce process development cycles by prototyping system parameters in a process recipe, or give experimentally validated physical models that can be used for optimization of existing systems.

Many research studies have focused on modeling transport mechanisms in single wafer rapid thermal processing (RTP) systems [7, 8, 9, 10, 11], where nonuniform heat transfer mechanisms can prevent across-wafer temperature uniformity during the process cycle. Typical modeling studies of RTP chemical vapor deposition systems include a gas phase transport submodel and a wafer submodel to account for the interactions between the gas phase and wafer itself. In addition to the dominant radiative energy exchange modes inside the chamber, it is often found that conductive heat loss from the wafer to the ad-

adjacent gas phase is important in determining wafer temperature in low pressure reactors [7, 12, 13, 14, 15]. However, the influence of reactant gas composition on wafer temperature through gas thermal conduction has not yet been widely studied; this is partly attributable to the difficulty of quantifying the thermal conduction flux when a simplified boundary condition (e.g. terms such as  $h(T_w - T_g)$ ) at the wafer/gas interface is used. Although a highly detailed, finely-discretized gas phase transport submodel with special attention focused on the gas/wafer boundary condition solved simultaneously with the wafer dynamical submodel can provide insightful information on the gas conductive effect, the intensive computational requirements of this numerical solution procedure usually limits the applicability of such an approach. As one example, previous research by Hasper *et. al.* [13] showed the gas conduction effect of pure hydrogen, argon, and a 50/50 hydrogen/argon mixture at different total pressures. Model predictions achieved very satisfactory agreement with experimental data for pure gases without parameter fitting, but the model predictivity was limited for gas mixtures because the lack of theoretical model parameter values for the gas mixtures.

In this paper, we continue our work [16] of developing a low-order gas/wafer heat transfer model with true predictive capabilities. The model accounts for gas flow across the wafer, the three dimensional gas temperature field, heat conduction within the wafer, and heat transfer between the wafer, gas, and reactor chamber. The gas temperature field submodel is solved using a global discretization method [17, 18], resulting in a relatively low order and computationally efficient simulation procedure. This model was used in an iterative, optimization-based parameter estimation procedure to determine a subset of the heat transfer parameters, using experimental measurements of wafer temperature as a function of gas composition. Additional experiments were conducted to show the minimal effect

*total* gas flow rate had on observed wafer temperature when gas composition was held constant. This verified the model prediction of the dominance of gas conductive heat transfer mechanisms relative to convective effects. What was produced was a validated process heat transfer model with relatively few adjustable parameters that gave valuable insight into the heat transfer mechanisms of this CVD system. The predictivity of this model can be used for developing a tighter temperature control system for this reactor [19] and for designing better conditioning procedures for process metrology [20].

## II. Experimental

Our research focuses on the ULVAC ERA-1000 selective tungsten deposition cluster tool, consisting of two single-wafer reactors joined by a buffer and a load-lock chamber for automatic loading and transfer of wafers. Figure 1 depicts the individual reactor configuration. Reactant gases are fed to the reactor from two sources: a gas mixture of silane and tungsten hexafluoride is injected through a two-dimensional nozzle installed on one side wall, and hydrogen is pumped in through a transparent showerhead mounted in the top of the reactor chamber. Gases mix in the chamber and react at the surface of a wafer located at the chamber center. For convenience we use 4 inch diameter wafers, although the tool is capable of processing 8 inch wafers. The wafer is supported by a slowly rotating 4 inch diameter quartz susceptor to assure the azimuthal symmetry of the deposited film. An incoherent tungsten-halogen lamp ring above and outside the reactor chamber is used to heat the wafer to  $400^{\circ}C$  through the transparent quartz showerhead window. Typical deposition runtimes last 5 minutes after operating temperature is reached.

A SensArray 1530 thermocouple (TC) wafer was used to measure the true wafer temperature, and the system was operated in I/O mode to enable manual loading/unloading of the

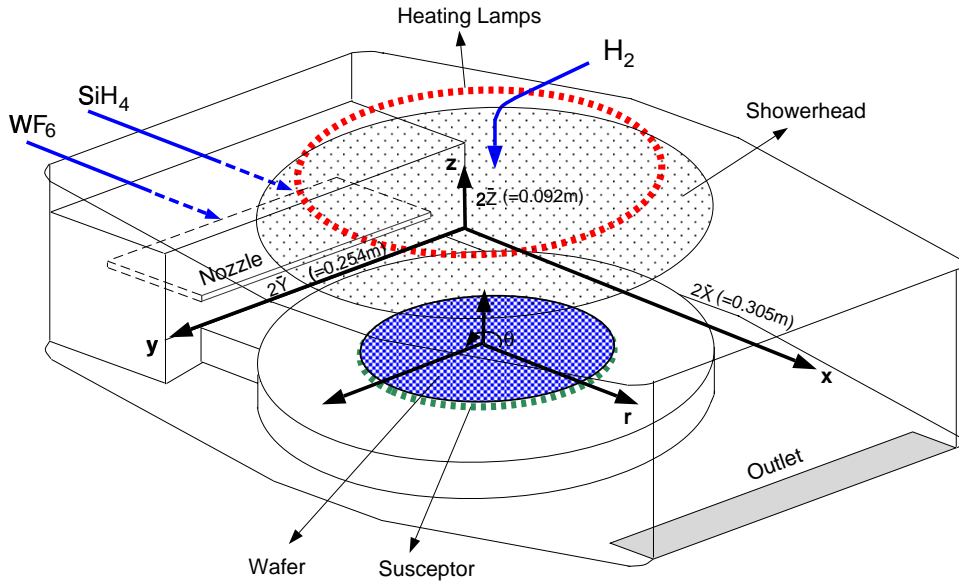


Figure 1: Sketch of the Tungsten CVD reactor system.

instrumented wafer. There are five thermocouples, labeled as shown in Figure 2, attached to the top surface of this instrumented TC wafer. We note that the instrumented wafer is designed to measure the *wafer* temperature - as opposed to wafer surface or thermocouple temperature - by bonding the thermocouple leads in an undercut wafer area in a symmetric pattern [21, 22]. A  $\pm 1.0$  °C or better measurement variation between these thermocouples has been reported [21, 22]. The thermocouple wafer was intentionally shifted about 3.8 cm from susceptor center in the downstream direction, and slightly rotated so that thermocouple 5 was not located on top of the susceptor (see Figure 2). This shifting was designed to study the conductive heat transfer from wafer to the underlying susceptor. The wafer rotation was turned off during the experiments to protect the leads of the test wafer.

The temperature data collected from the instrumented wafer was sent to a personal computer based data acquisition system that included a LabView software interface and two computer boards: a CIO-DAS801 data acquisition board [23] and a CIO-EXP32 extension board [24]. Each thermocouple was connected to a channel on the expansion board, where

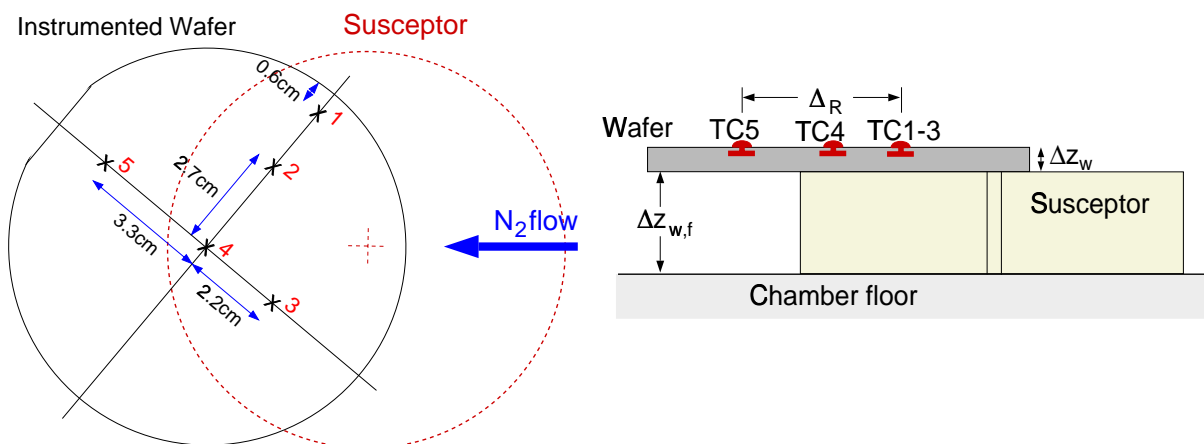


Figure 2: The top and side views of the test wafer position with thermocouple positions marked.

a low pass filter with bandwidth 7 Hz was implemented between the high and low ends and a 100  $k\Omega$  resistor was installed between low and ground to provide ground reference. The temperature signals were then amplified 300-fold before being sent to the data acquisition board. An on-board semiconductor sensor provides the adjustable cold junction compensation (CJC) function that subsequently is used as a reference to the measured thermocouple signals in the LabView program. Additional processing variables of ULVAC CVD system, such as the system thermocouple temperature measured near the lamp, lamp power control signal, chamber pressure, and gas feed rates, are collected during the processing cycle. The sampling rate selected was 20  $Hz$ .

Two sets of experiments were conducted to investigate the influence of gas composition and total flow rate on wafer temperature in the ULVAC system. The first experiment, designed to study the effect of gas mixture composition at constant total flow rate, began by changing the initial reactant gases feed rates of 100  $sccm$  pure hydrogen (Case 1), to several different combinations: Case 2: 80  $sccm$   $H_2$ /20  $sccm$   $N_2$ ; Case 3: 60  $sccm$   $H_2$ /40  $sccm$   $N_2$ ; Case 4: 40  $sccm$   $H_2$ /60  $sccm$   $N_2$ ; and Case 5: 100  $sccm$   $N_2$ . The gas flow rates/composition were changed only after the instrumented wafer temperature

reached steady-state in each period (approximately 20 minutes). The wafer temperature set point and chamber pressure were maintained at 500 °C and 500 *mTorr* throughout the experiments. The lamp power was observed to remain constant after the initial fast ramp-up despite the true wafer temperature variations attributable to the changes in gas composition, as shown in Figure 3. This lack of movement of the system controller to compensate for true wafer temperature losses can be understood in terms of the following two reasons: first, the system thermocouple is located outside the reactor chamber, thus any gas composition change will have no effect on its temperature measurement; second, the fixed look-up table, designed to factor in the feed gas flows and chamber pressure when converting system thermocouple temperature to wafer temperature, was inactive in the I/O operation mode. Therefore, the system wafer temperature used as the feedback signal in the temperature control loop remained constant, producing no net set-point deviation. Detailed discussions regarding the ULVAC temperature control system can be found in [19].

The wafer temperature time histories for the first experiment are shown in Figure 3. The wafer temperature indicated by the ULVAC control system (measured by the lamp thermocouple) is also plotted for reference. Generally, the steady-state wafer temperature was found to be lower in pure hydrogen than for pure nitrogen, and it gradually increased with nitrogen fraction. Because the lamp power output was maintained at a constant level, these temperature differences are due to the changing gas mixture properties, most importantly the gas thermal conductivity: we note that the pure hydrogen thermal conductivity is about six times larger than that of nitrogen at 500 *mTorr*. This gas property-related temperature difference is more significant in the measurement of TC No. 5, where the back-side of the wafer contacts reactant gas instead of the quartz susceptor. The temperature deviation of TC No. 4 from TC No. 1-3 is due to the positioning of TC No. 4, which is



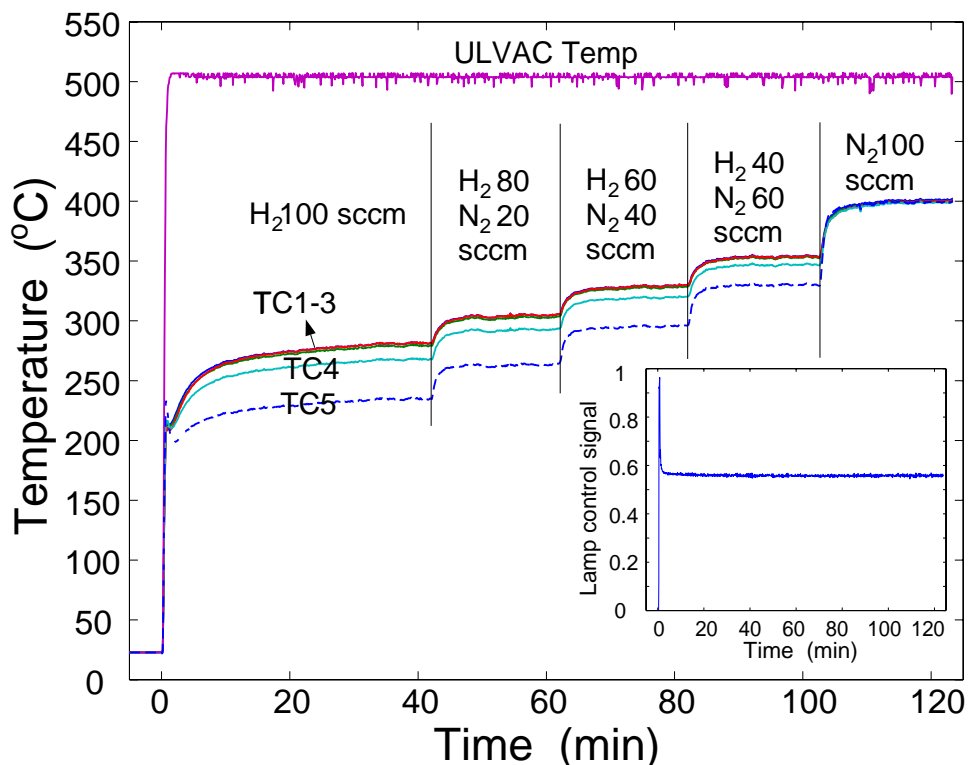


Figure 3: The temperature response of the wafer to reactant gas composition variations.

close to the susceptor edge and is affected by the edge heat loss of the susceptor.

The second experiment was designed to study the effect of gas bulk velocity on wafer temperature, as well as to verify the observations made in the first experiment. In this experimental sequence, wafer heating was begun in pure nitrogen, and the compositional and total flow rates were changed according to Case 1: 100 *sccm*  $N_2$ ; Case 2: 60 *sccm*  $N_2$ ; Case 3: 40 *sccm*  $H_2$ /60 *sccm*  $N_2$ ; Case 4: 40 *sccm*  $H_2$ ; and Case 5: 100 *sccm*  $H_2$ . The experimental results are plotted in Figure 4. We note that when the wafer temperature responses are compared for the different flow rates of Case 1 and 2 in pure nitrogen, as well as 4 and 5 in pure hydrogen, only insignificant differences were observed. *This result indicates the gas convective heat transfer modeling terms can be neglected in the low pressure processing condition of the ULVAC system.* Also, by comparing the temperature measurements of the second experiment to the first one at three different gas compositions (100 *sccm*  $N_2$ ,

60 *sccm*  $N_2$ /40 *sccm*  $H_2$ , and 100 *sccm*  $H_2$ .) the temperature differences are found to be less than 5 °C for pure nitrogen gas flow and are almost equal in the other two cases, demonstrating the repeatability of the experiments. In addition, it should be noted that the TC No. 5 measurement, represented as the dashed curve, responded faster during the initial heating ramp phase while the other thermocouples, positioned in the wafer area above the susceptor, showed slower temperature increases due to the additional energy absorbed by the underlying susceptor during the ramp-up phase.

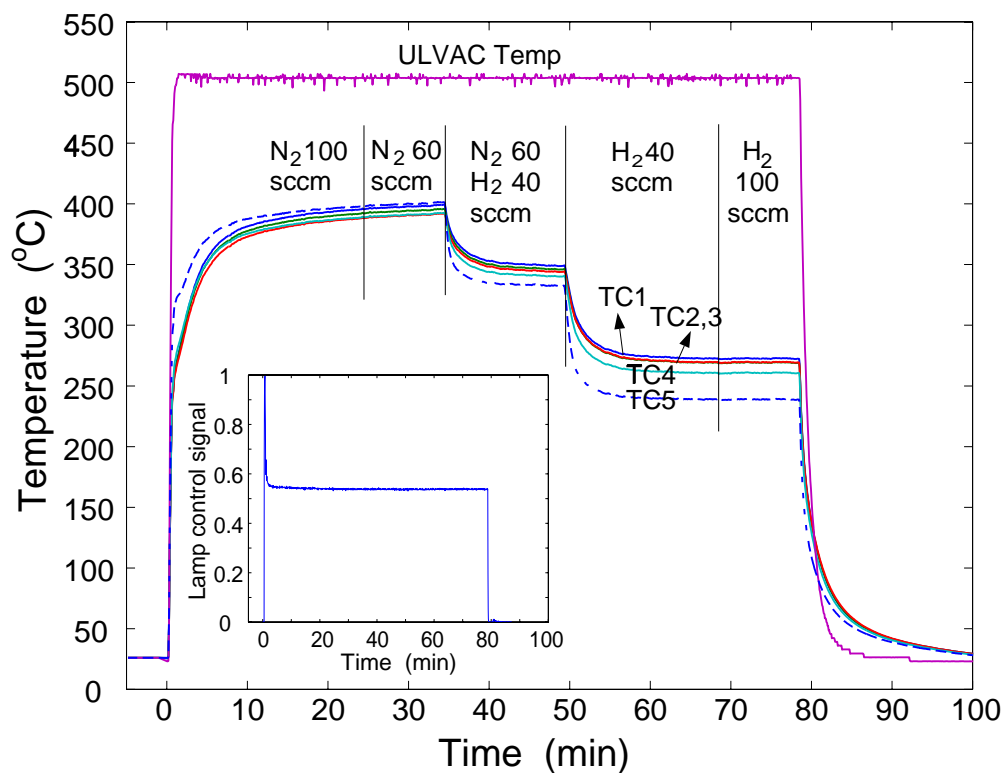


Figure 4: The temperature response of the wafer to reactant gas flow rate and composition changes.

### III. Mathematical Model

An integrated model of the ULVAC tungsten CVD system has been developed that describes the interactions between gas phase velocity and temperature fields and the wafer thermal

dynamics. The coordinates of gas phase and wafer computational domain are defined in Figure 1. In the case of pure nitrogen flow, gas enters only through the side wall nozzle. For the operating conditions used in the experimented study, we should not expect turbulent or bouyancy-induced convective mixing effects [16]; therefore the gas will flow horizontally over the wafer for the pure nitrogen case (the case of nonzero hydrogen flow will be discussed later in the paper.) The fully developed, laminar velocity profile is described by the continuity and steady state Navier-Stokes equations

$$\frac{\partial v_x}{\partial x} = 0 \quad (1)$$

$$\frac{\partial^2 v_x}{\partial y^2} + \alpha_v \frac{\partial^2 v_x}{\partial z^2} = \beta_v \quad (2)$$

subject to no-slip boundary conditions at  $y = 0, 1$  and  $z = 0, 1$ .

Because of the short residence time relative to wafer thermal dynamics, the gas temperature can be described by the steady-state conservation of energy

$$v_x \frac{\partial T_g}{\partial x} = \left( \delta_{gt} \frac{\partial^2}{\partial x^2} + \beta_{gt} \frac{\partial^2}{\partial y^2} + \gamma_{gt} \frac{\partial^2}{\partial z^2} \right) T_g = \mathcal{L}T_g. \quad (3)$$

Gas inlet temperature is assumed equal to the water-cooled chamber wall temperature; a zero gradient along flow direction boundary condition is used at the gas outlet. Gas temperature is set equal to showerhead and wafer temperature inside the relative areas at the top and bottom chamber surfaces. Overall, this gives the gas temperature boundary conditions:

$$T_g = 0 \quad \text{at } x = 0,$$

$$\frac{\partial T_g}{\partial x} = 0 \quad \text{at } x = 1,$$

$$\begin{aligned}
T_g &= C_1(T_{wall}^*) \quad \text{at } y = 0, 1, \\
T_g &= \begin{cases} C_t(T_{sh}^*) & \text{at } z = 1, \quad (x - 0.5)^2 + R_{xy}^2(y - 0.5)^2 \leq R_t^2, \\ 0 & \text{at } z = 1, \quad (x - 0.5)^2 + R_{xy}^2(y - 0.5)^2 > R_t^2, \end{cases} \\
T_g &= \begin{cases} C_b(T_w^*) & \text{at } z = 0, \quad (x - 0.5)^2 + R_{xy}^2(y - 0.5)^2 \leq R_b^2, \\ 0 & \text{at } z = 0, \quad (x - 0.5)^2 + R_{xy}^2(y - 0.5)^2 > R_b^2. \end{cases} \quad (4)
\end{aligned}$$

The dimensionless parameters and variables are defined in Table 1. The gas mixture density  $\rho$ , thermal conductivity  $\kappa$ , heat capacity  $C_p$ , and viscosity  $\mu$  are determined from mixture-averaged properties [25] and the pure species viscosities are calculated from the kinetic theory of gases at the reference temperature  $T_{amb} = 298K$ .

Table 1: Definitions of dimensionless variables and parameters. The dimensional quantities are marked with a \*.

Dimensionless variables	Dimensionless parameters
$x = x^*/2\bar{X}$	$\alpha_v = \bar{Y}^2/\bar{Z}^2$
$y = y^*/2\bar{Y}$	$\beta_v = 2\mathcal{P}\bar{Y}^2/(\mu < v > \bar{X})$
$z = z^*/2\bar{Z}$	$\alpha_{gt} = \kappa/(\rho C_p)$
$v_x = v_x^*/< v >$	$\delta_{gt} = \alpha_{gt}/(2 < v > \bar{X})$
$T_g = (T_g^* - T_{amb})/T_{amb}$	$\beta_{gt} = \alpha_{gt}\bar{X}/(2 < v > \bar{Y}^2)$
	$\gamma_{gt} = \alpha_{gt}\bar{X}/(2 < v > \bar{Z}^2)$
	$C_t = (T_{sh}^* - T_{amb})/T_{amb}$
	$C_b = (T_w^* - T_{amb})/T_{amb}$
	$R_{xy} = \bar{Y}/\bar{X}$
	$R_t = R_{sh}/2\bar{X}$
	$R_b = R_w/2\bar{X}$

## A. Wafer Thermal Dynamics Model

The one-dimensional wafer thermal dynamics model can be written as follows,

$$\Delta_{Z_w} \rho_w \frac{\partial (C_{pw} T_w)}{\partial t} = \Delta_{Z_w} \kappa_w \nabla^2 T_w + Q_{lamp} + Q_{rad} + Q_{top} + Q_{bot} \quad (5)$$

where the energy fluxes from the lamp heating, radiation loss, convective/conductive losses from wafer top, and conduction loss from wafer bottom are defined as

$$\begin{aligned}
Q_{lamp} &= \alpha_w(T_w)Q_{lp}u(t) \\
Q_{rad} &= -\frac{F_{A,top}\sigma(T_w^4 - T_{sh}^4)}{\epsilon_w^{-1}(T_w) + \epsilon_{sh}^{-1}(T_{sh}) - 1} - \frac{F_{A,bot}\sigma(T_w^4 - T_f^4)}{\epsilon_w^{-1}(T_w) + \epsilon_f^{-1}(T_f) - 1} \\
Q_{top} &= \kappa_g(T_{w,z=0})\frac{\partial T_{g,z=0}}{\partial z} \\
Q_{bot} &= -h_{eff}(T_w)(T_w - T_f).
\end{aligned} \tag{6}$$

In the model, the subscripts  $w$ ,  $sh$ , and  $f$  represent the state variables or physical properties corresponding to the wafer, showerhead, and chamber floor, respectively.  $\Delta_{z_w}$  is the wafer thickness,  $\sigma$  is the Boltzmann constant, and  $F_A$  is the geometric factor that is equal to 1 for both wafer top and bottom surfaces [26].  $h_{eff}$  is an effective heat transfer coefficient,  $Q_{lp}$  is the incident lamp bank emissive power at the wafer surface, and  $u(t)$  is dimensionless time-dependent lamp control signal recorded from the experiments.  $\epsilon$  is the temperature-dependent total emissivity interpolated from data points of silicon [27] and quartz [10] for the wafer and showerhead, respectively. A constant emissivity of 0.26 is used for the cooled, oxidized aluminium chamber wall and floor. The wafer absorptivity  $\alpha_w$  is assumed equal to the emissivity of silicon [28].

To describe the across-wafer temperature variations observed in our experimental data, we use different steady-state modeling approaches for wafer areas located above and beyond the susceptor outer edge. For the wafer region positioned above the susceptor (TC No.1-3), the governing equation (5) at steady-state becomes

$$Q_{lamp} + Q_{rad} + Q_{top} + Q_{bot} = 0. \tag{7}$$

The value of  $Q_{top}$  is computed by numerically differentiating the gas temperature at wafer/gas boundary as described in equation (6). Because the wafer is not clamped against the susceptor, there is no real solid-solid contact [13], and therefore an effective heat transfer coefficient  $h_{eff}$  is used to approximate the combined heat transfer between wafer backside surface and chamber floor. This empirical, temperature-dependent heat transfer coefficient can be approximated by

$$h_{eff}(T_w) = h_{eff,0} + \alpha_0(T_w - T_{w,N_2}),$$

which includes the nominal heat transfer coefficient  $h_{eff,0}$  and constant of proportionality  $\alpha_0$ , that must be determined by fitting the experimental data to the model. Modeling the heat transfer in this form is equivalent to the Taylor's series expansion of the true function, evaluated at  $T_{w,N_2}$ . The wafer thermal conduction term  $\Delta_{Z_w} \kappa_w \nabla^2 T_w$  is neglected because the averaged wafer temperature measurement from thermocouples No. 1-3 is used for data analysis. However, this conduction term proves to be small compared to other energy transfer mechanisms when estimated for the TC No. 5 location and we should expect even smaller amount of energy conducted for measurement points above the susceptor. Temperature data from thermocouple No. 4 is not considered here because it is affected by the susceptor edge heat transfer.

In the wafer region where thermocouple No. 5 is located, the wafer backside surface is in contact with reactant gas. The steady-state model takes the form

$$Q_{cond} + Q_{lamp} + Q_{rad} + Q_{top} + Q_{bot} = 0. \quad (8)$$

$Q_{cond}$  is approximated using finite-difference formula

$$Q_{cond} \approx \Delta_{Z_w} \kappa_w(T_{w,5}) \left[ \frac{\bar{T}_{w,1-3} - T_{w,5}}{\Delta_R} - 0 \right] / \Delta_R$$

where  $\Delta_R$  is the distance between thermocouple No. 5 and the averaged position of thermocouples No. 1-3.

Under low pressure processing conditions, the heat conduction between two parallel solid surfaces is proportional to the molecular mean free path in the gas phase. Because the gap distance between wafer and chamber floor is comparable to the gas molecular mean free path in the ULVAC system, the continuum flow model of the heat transfer must be modified and the correction of heat transfer coefficient is expressed as [13, 14]

$$h_{eff} \approx \frac{\kappa_g}{\Delta_{Z_{w,f}} + 2\beta_{w,f}\lambda} \quad (9)$$

where  $\kappa_g$  is the mean thermal conductivity evaluated at  $\bar{T}_{w,f} = (T_w + T_f)/2$ ,  $\Delta_{Z_{w,f}}$  is the wafer-floor gap distance, and  $\lambda$  is the mean free path defined by gas mixture molecular weight  $M$ , viscosity, and pressure  $p$  [25] as

$$\lambda = 3.2 \frac{\mu}{p} \left( \frac{R\bar{T}_{w,f}}{2\pi M} \right)^{1/2}.$$

The constant  $\beta_{w,f}$  is defined by thermal accommodation coefficient  $\alpha$  and the ratio of specific heats  $\gamma = C_p/C_v$  at constant pressure and volume [13, 14]

$$\beta_{w,f} = \frac{2 - \alpha}{\alpha} \frac{9\gamma - 5}{2\gamma + 2},$$

and is on the order of unity.

**B. Parameter Estimation**

There are several parameters in the wafer energy balance model for which values are difficult to compute accurately using published correlations or other *a priori* approaches. The lamp radiant flux intensity at the wafer surface,  $Q_{lp}$ , depends on the true emissive power of the heating lamps, the geometry of the reactor and chamber walls, and the adsorption characteristics of the quartz showerhead window. The upper limit of  $Q_{lp}$  of the ULVAC system, however, can be estimated by dividing the product of measured maximum lamp current and voltage by an approximated 0.3 m diameter circular area of the chamber floor.

The thermal accommodation coefficient  $\alpha$ , used to define the constant  $\beta_{w,f}$  in the conductive flux relation for the thin gas gap between the wafer and chamber floor, can deviate from the theoretical value calculated using the hard sphere molecular collision assumption [13]. Here we take the approach of Kleijn and Werner [14] to estimate the value of  $\beta_{w,f}$  instead. As discussed in the previous section, the temperature dependent heat transfer coefficient  $h_{eff}$  must also be identified by using experimental measurement to accommodate the overall heat transfer coefficient that combines thermal conduction from wafer to susceptor, thermal conduction across the susceptor, and reactant gas thermal conduction between susceptor and chamber floor. The representative guide values of the system parameters to be estimated are listed in Table 2 for reference.

Table 2: A list of model parameter values, their estimated values or range, and the final values obtained from the identification procedure.

Variables	Guide values	Reference	Values identified in this study
$Q_{lp}$	46740 $W/m^2$	Maximum value	30341.6 $W/m^2$
$\beta_{w,f}$	$\approx 1$	[14] (Theoretical value)	17.820
	30	[14] (Estimated value)	
$h_{eff,0}$	$> 0$		3.409 $W/(m^2K)$
$\alpha_0$	$\alpha_0 < h_{eff,0}/(120K)$		-0.048 $W/(m^2K^2)$



### C. Solution Procedure

To estimate the system parameters  $Q_{lp}$ ,  $\beta_{w,f}$ ,  $h_{eff,0}$ , and  $\alpha_0$ , we developed an iterative solution procedure that solves equations (1)-(6) to resolve the interactions at the wafer/gas phase boundary. The overall solution algorithm begins by using the gas composition and measured wafer temperature to compute corresponding physical properties and to set the flow velocity and temperature field boundary conditions. The gas flow velocity field is computed using a Galerkin discretization technique [16] based on globally defined eigenfunctions; this solution approach determines the flow velocity component  $v_x$  and the pressure drop term  $\beta_{gt}$ .

By defining the gas temperature as a linear combination of gas temperature inside the gas domain ( $T_\Omega$ ) and at the chamber top and bottom boundaries ( $T_{\partial\Omega,t}$ ,  $T_{\partial\Omega,b}$ ),

$$\begin{aligned} T_g &= T_\Omega + T_{\partial\Omega,t} + T_{\partial\Omega,b} \\ &= \sum_{l,m,n=1}^{L,M,N} b_{lmn} \phi_l(x) \psi_m(y) \zeta_n(z) + \sum_{l,m=1}^{L,M} a_{lm} \phi_l(x) \psi_m(y) z + \sum_{l,m=1}^{L,M} d_{lm} \phi_l(x) \psi_m(y) (1-z), \end{aligned} \quad (10)$$

we can formulate the residual of the gas temperature equation by substituting the corresponding trial function expansions into equation (3) to define the residual function

$$\mathcal{R} = \mathcal{L}T_\Omega + \mathcal{L}(T_{\partial\Omega,t} + T_{\partial\Omega,b}) - v_x \frac{\partial T_g}{\partial x}. \quad (11)$$

In equation (11) the  $b_{lmn}$ ,  $a_{lm}$ , and  $d_{lm}$  are mode amplitude coefficients, and  $\phi_l$ ,  $\psi_m$ , and  $\zeta_n$  are eigenfunctions in the three physical directions that satisfy  $\mathcal{L}\phi\psi\zeta = \lambda\phi\psi\zeta$  and the homogeneous form of boundary conditions (4). The values of  $a_{lm}$  and  $d_{lm}$  are computed by projecting the gas temperature boundary conditions at  $z = 0, 1$  onto (11). The residual

function (11) is then projected onto the eigenfunctions using Galerkin's method. Because the eigenfunctions are defined by the eigenvalue problem  $\mathcal{L}\phi\psi\zeta = \lambda\phi\psi\zeta$ , we simplify the first term in (11) by replacing it with  $\sum_{l,m,n=1}^{L,M,N} \lambda_{lmn} \overline{b_{lmn}} \phi_l \psi_m \zeta_n$ .

Because of the relative minor contribution of the convective term  $v_x \partial T_g / \partial x$ , the mode amplitude coefficients can be determined by the convergent, iterative algorithm:

$$b_{i,j,k} = \left\langle \mathcal{L}(T_{\partial\Omega,t} + T_{\partial\Omega,b}) - v_x \frac{\partial T_g}{\partial x}, \phi_i \psi_j \zeta_k \right\rangle / \lambda_{i,j,k}. \quad (12)$$

The weighted inner product is defined as

$$\langle f, g \rangle = \int_0^1 \int_0^1 \int_0^1 f g \, dx dy dz.$$

The representative gas temperature contours and wafer/gas energy transfer rate are displayed in Figure 5 for the simulation condition corresponding 100 *sccm*  $N_2$ .

Taking the wafer-average gas/wafer heat transfer rate (Figure 5(b)) as the  $Q_{top}$  in equation (6), we compute the wafer temperature using Newton's method to solve equation (7) for the TC No. 1-3 region and (8) for the TC No. 5 region. The updated wafer temperature is then fed back to the gas temperature computation as a new boundary condition at the chamber floor, and the entire computation is performed again. This iterative wafer temperature computation scheme stops when a pre-specified temperature error tolerance is satisfied.

The parameter estimation procedure is based on minimizing the sum of the squared errors (SSE), where the error is defined by the difference between the experimentally measured and predicted wafer temperature at each gas composition. A MATLAB optimization toolbox function `minsearch.m` is used for this parameter identification method. The total

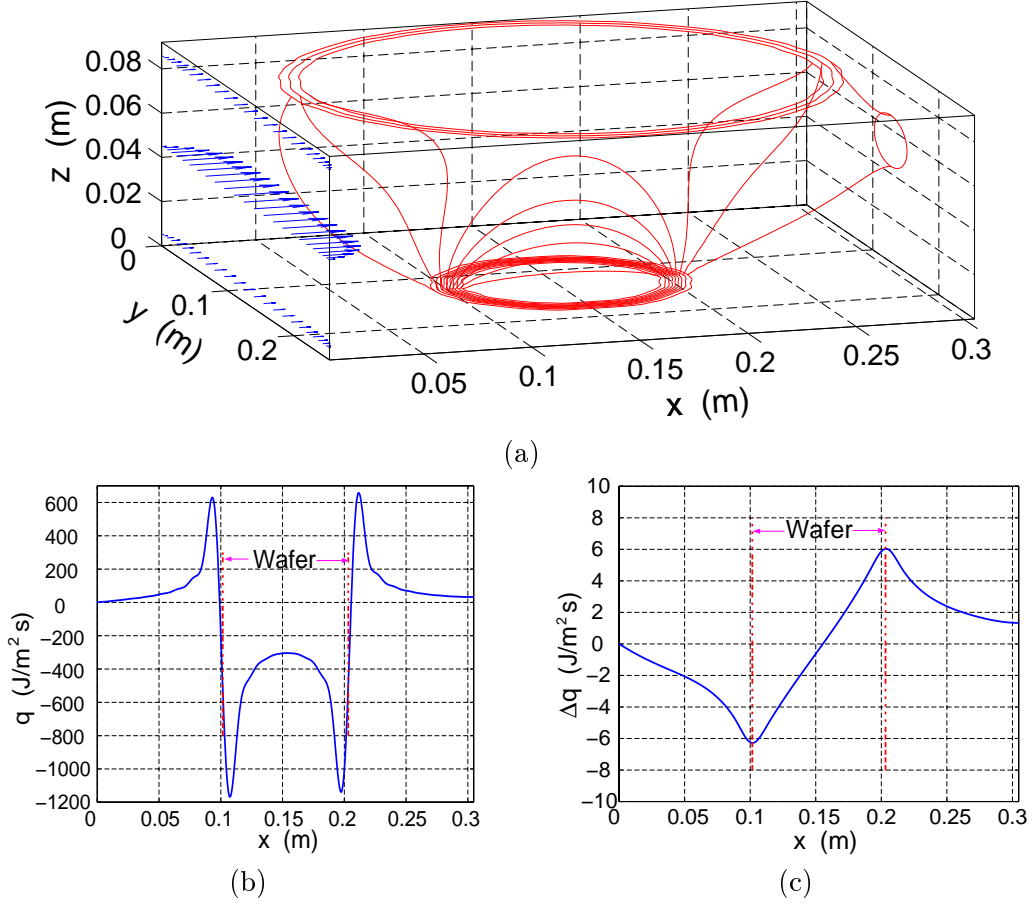


Figure 5: (a) Gas flow field and temperature contours where each contour represents 50  $K$  temperature difference. (b) Wafer/gas heat transfer rate at centerline of the reactor chamber. Simulation performed at  $N_2 = 100$  *sccm* and 500 *mTorr*. (c) Difference of heat flux across wafer/gas boundary between  $N_2 = 100$  and 60 *sccm*, where  $\Delta q = q_{N_2=100} - q_{N_2=60}$ .

identification procedure consists of the two optimization substeps:

1. Estimate the values of  $Q_{lp}$  and  $\beta_{w,f}$  by minimizing the objective function defined by temperature data from TC No. 5.
2. Using the value of  $Q_{lp}$  estimated in first step, calculate the effective heat transfer coefficient parameters  $h_{eff,0}$  and  $\alpha_0$  based on the minimizing the objective function defined by mean temperature measurement of TC No. 1-3.

The empirical showerhead temperature  $T_{sh}$  and floor temperature under the wafer  $T_f$  are

assumed to be a constant  $150\text{ }^{\circ}\text{C}$  and  $60\text{ }^{\circ}\text{C}$  at steady-state, respectively. These values were obtained after a number of parameter identification runs and are consistent with observations made during the experiments. Figure 6 shows the steady-state temperature measurements taken from Figure 3; an extra wafer temperature point at 20% hydrogen was interpolated and used along with these measurements in the parameter estimation procedure. The estimated results are listed in Table 2.

#### IV. Model Validation and Discussion

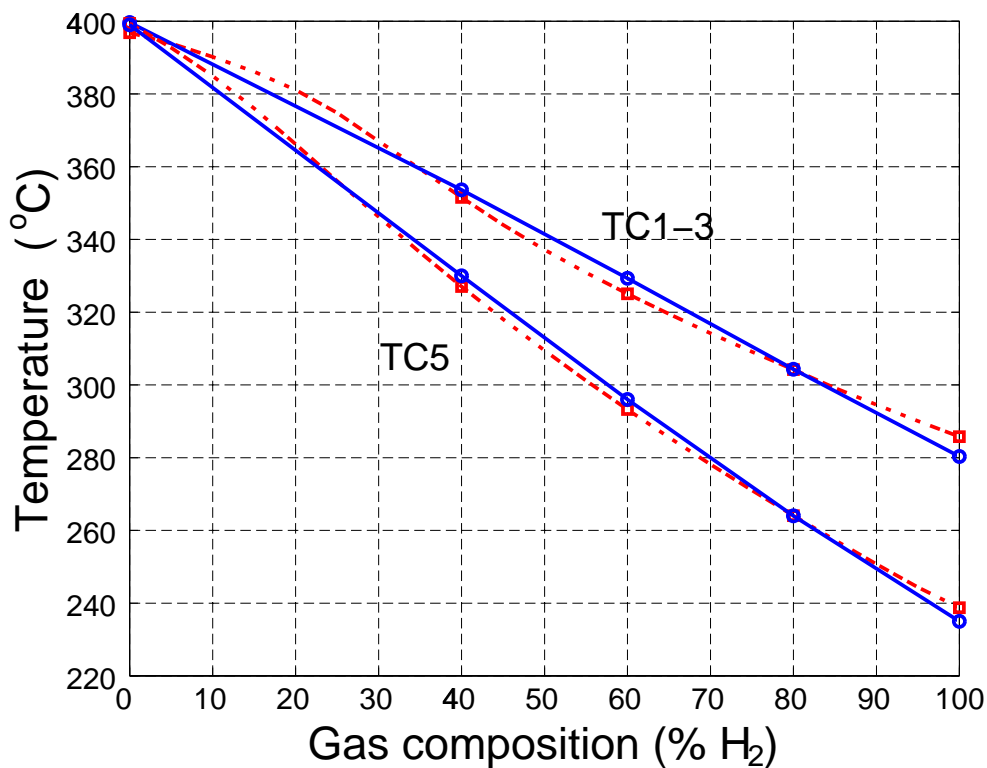


Figure 6: Wafer temperature from experimental data (solid curves with circles at data points) and model prediction (dot-dash curves and squares).

We approach the problem of assessing the validity of our CVD simulator from two directions. The first test consists of a direct comparison of the model predictions over the entire gas composition range to the interpolated experimental data curves. Because the observed

wafer temperatures demonstrate a nearly linear correlation with gas  $H_2$  fraction, this test provides a good indication of whether the model structure and parameter values correctly reflect the balance between the highly nonlinear contributions of radiative heat transfer terms and the composition-dependent heat transfer mechanisms. Comparing the model predictions and experimental data reveals a mean model prediction error of less than 3 K for each data set (Figure 6). The heat transfer contributions from each terms in equation (6) are plotted in Figure 7. In both wafer regions, the radiative heat fluxes ( $Q_{lamp}$  and  $Q_{rad}$ ) dominate in the high temperature range ( $> 300\text{ }^\circ C$ ) and show nonlinear variations relative to the other heat transfer mechanisms because of the temperature dependency of wafer emissivity (absorptivity). The heat loss from  $Q_{bot}$ , which is more significant in the wafer area outside the susceptor (Figure 7(b)), increases in higher hydrogen fractions due to gas thermal conductivity increases and becomes equivalent to wafer irradiation around  $300\text{ }^\circ C$  (corresponding to 80%  $H_2$  in Figure 7(a) and 60%  $H_2$  in (b)). The thermal conduction through the wafer resulting from wafer temperature nonuniformity is negligible (Figure 7(b)), justifying our decision to ignore this term in the more temperature-uniform wafer interior region.

As the second test of model validity, we compare identified parameter values to values used in other studies, or compare our identified values to a range of values that can be theoretically justified. The guide and identified parameter values are compared in Table 2. The system dependent maximum incident lamp radiant flux  $Q_{lp}$ , as computed in previous section, is found to be about 1.5 times the value we estimated. The constant parameter  $\beta_{w,f}$ , on the other hand, is an order of magnitude larger than the theoretical value, but it is close to the value that was identified by Kleijn and Werner [14] using data obtained from their low pressure CVD reactor. Finally, the overall wafer/chamber floor heat transfer

coefficient must be positive. Because  $T_w - T_{w,N_2} < 0$ , the requirement  $h_{eff} > 0$  translates into an upper limit of  $\alpha_0$  as defined in Table 2; we note that the identified value satisfies this condition.

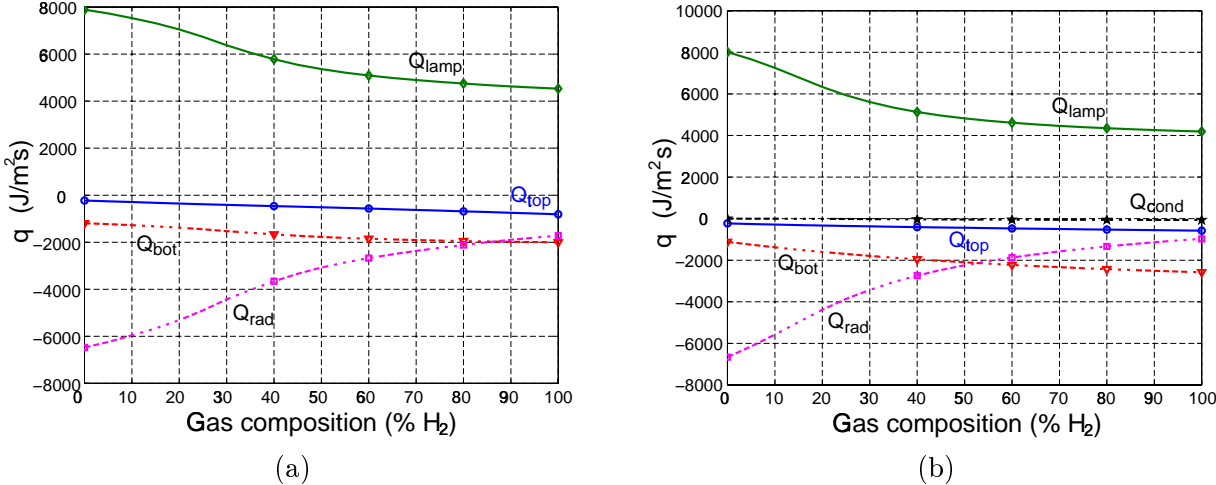


Figure 7: Contributions of individual heat transfer mechanisms for (a) interior region, and (b) region outside the susceptor.

### A. Solution Insensitivity to Flow Field

In Figure 5(c), we compare predicted gas/wafer heat transfer rates at 100 and 60 *scm* nitrogen gas flows, corresponding to the experimental conditions used in Figure 4. While these simulations are computed based on the averaged thermocouple temperature measurements of TC No. 1-3, similar results are obtained when TC No. 5 measurements are used in the computation. The differences of the energy flux across the wafer/gas boundary of both gas flow cases are less than  $7 \text{ W}/(\text{m}^2\text{K})$  and are small compared to the magnitude of the gas heat transfer rate itself. These simulation results corroborate with also supports our experimental observations that the convective heat transfer effects are negligible when compared to gas conduction. The combination of the model predictions and experimen-

tal observations of the relative insensitivity of the wafer temperature to the gas velocity field justifies our omission of detailed fluid flow simulations of the combined side inlet and showerhead inlet streams.

## B. Extrapolation of Model Predictions

The validated model predictions can be directly or indirectly extrapolated to actual processing condition. For example, because the convective heat transfer has only an insignificant effect on the wafer temperature, we can expect our wafer temperature predictions will not be affected by the 4 rpm wafer rotation used during process operation.

The use of the instrumented wafer limited experimental observations to tests only with non-reacting gas species. However, because wafer temperature was directly correlated to gas thermal conductivity in our modeling work, the results can be directly extrapolated to process gases containing  $WF_6$  and  $H_2$  and/or  $SiH_4$  with adjustments made to wafer emissivity due to the deposited tungsten film. Our current blanket tungsten deposition processing recipe [20] consists of 10 *sccm*  $WF_6$  and 40 *sccm*  $H_2$  with a 15 to 20 minutes pre-conditioning period; our simulation predicts  $T_w = 322\text{ }^\circ C$  at the start of deposition.

## V. Conclusions

The primary objective of this work was to study the influence of reactant gas composition on wafer temperature in a single-wafer CVD system. Both experimental observations and simulation studies showed the wafer temperature was a strong function of the wafer/gas interface thermal conduction compositional dependency; however, gas convective heat transfer mechanisms only had minimal effect on the wafer temperature. Good agreement was found between the model predictions and experimental data at various gas compositions, and the

estimated parameter values were justified when compared with their guide values.

An important result of this experimental and simulation work was the validation of the theoretical predictions of previous modeling work [16]. In the cited paper, the minor contributions of convective gas phase transport mechanisms and gas phase nonlinearities (e.g., those important in higher-pressure systems, such as [29, 30, 31]) were predicted for this low-pressure reactor system. Therefore, for the W CVD system studied in this work, a global spectral method approach was chosen over finite element and other localized discretization techniques. This choice was made to take advantage of the simplicity with which the global projection method could be implemented, allowing the researchers to focus on identifying the most important heat transfer modes in the system through an iterative parameter identification method.

## VI. Acknowledgments

The authors wish to gratefully thank T. Gougousi, L. Henn-Lecordier and Y. Xu for their technical support during the experimental work. HYC acknowledge partial support of the Small Sensor Systems Center of the University of Maryland.

## References

- [1] B. Peuse, G. Miner, M. Yam, and C. Elia. Advances in RTP temperature measurement and control. In M. C. Ozturk, F. Roozeboom, P. T. Timans, and S. H. Pas, editors, *Rapid Thermal and Integrated Processing VII*, volume 525 of *Mat. Res. Soc. Symp. Proc.*, pages 71–85, Warrendale, PA, 1998. Materials Research Society.



- [2] P. Vandenabeele and W. Renken. Model based temperature control in RTP yielding  $\pm 0.1^{\circ}\text{C}$  accuracy on a  $1000^{\circ}\text{C}$ , 2 second,  $100^{\circ}\text{C}/\text{s}$  spike anneal. In M. C. Ozturk, F. Roozeboom, P. T. Timans, and S. H. Pas, editors, *Rapid Thermal and Integrated Processing VII*, volume 525 of *Mat. Res. Soc. Symp. Proc.*, pages 109–114, Warrendale, PA, 1998. Materials Research Society.
- [3] K. Tsakalis and K. Stoddard. Integrated identification and control for diffusion/CVD furnaces. In *6th IEEE Int. Conference on Emerging Technologies and Factory Automation*, pages 514–519, 1997.
- [4] T. S. Cale, P. E. Crouch, L. Song, and K. S. Tsakalis. Increasing throughput in low pressure chemical vapor deposition: An optimal control approach. In *Proceedings of American Control Conference*, pages 1289–1293, Seattle, WA, June 1995.
- [5] C. D. Schaper, M. M. Moslehi, K. C. Sarawat, and T. Kailath. Modeling, identification, and control of rapid thermal processing system. *J. Electrochem. Soc.*, 141(11):3200–3209, 1994.
- [6] J. D. Stuber, I. Trachtenberg, T. F. Edgar, J.K. Elliott, and T. Breedijk. Model-based control of rapid thermal processes. In *Proceedings of the 33rd Conference on Decision and Control*, pages 79–85, Lake Buena Vista, FL, December 1994.
- [7] H. A. Lord. Thermal and stress analysis of semiconductor wafers in a rapid thermal processing oven. *IEEE Transactions on Semiconductor Manufacturing*, 1(3):105–114, 1988.
- [8] C. R. Klijn, C. J. Hoogendoorn, A. Hasper, J. Holleman, and J. Middelhoek. Transport phenomena in tungsten LPCVD in a single-wafer reactor. *J. Electrochem. Soc.*,

- 138(2):509–517, 1991.
- [9] C. D. Schaper, Y. M. Cho, and T. Kailath. Low-order modeling and dynamic characterization of rapid thermal processing. *Appl. Phys. A*, 54:317–326, 1992.
- [10] J.-M. Dilhac, N. Nolhier, C. Ganibal, and C. Zanchi. Thermal modeling of a wafer in a rapid thermal processor. *IEEE Transactions on Semiconductor Manufacturing*, 8(4):432–439, 1995.
- [11] C. D. Schaper and T. Kailath. Thermal model validation for rapid thermal chemical vapor deposition of polysilicon. *J. Electrochem. Soc.*, 143(1):374–381, 1996.
- [12] S. A. Campbell, K.-H. Ahn, K. L. Knutson, B. Y. H. Liu, and J. D. Leighton. Steady-state thermal uniformity and gas flow patterns in a rapid thermal processing chamber. *IEEE Transactions on Semiconductor Manufacturing*, 4(1):14–19, 1991.
- [13] A. Hasper, J. E. J. Schmitz, J. Holleman, and J. F. Verwey. Heat transport in cold-wall single-wafer low pressure chemical-vapor-deposition reactors. *J. Vac. Sci. Technol. A*, 10(5):3193–3202, 1992.
- [14] C. R. Kleijn and C. Werner. *Modeling of Chemical Vapor Deposition of Tungsten Films*. Birkhauser Verlag, Boston, MA, 1993.
- [15] C. R. Kleijn. Chemical vapor deposition processes. In M. Meyyappan, editor, *Computational Modeling in Semiconductor Processing*, chapter 4. Artech House, Boston, 1995.
- [16] H.-Y. Chang and R. A. Adomaitis. Analysis of heat transfer in a chemical vapor deposition reactor: An eigenfunction expansion solution approach. *Int. J. Heat Fluid Flow*, 20:74–83, 1999.

- [17] Y. h. Lin, H.-Y. Chang, and R. A. Adomaitis. MWRtools: A library for weighted residual method computations. *Computers and Chemical Engineering*, 23:1041–1061, 1999. also in ISR TR 98-24.
- [18] R. A. Adomaitis, Y. h. Lin, and H.-Y. Chang. A computational framework for boundary-value problem based simulations. *Simulation*, 74:30–40, 2000. also in ISR TR 98-41.
- [19] H.-Y. Chang and R. A. Adomaitis. Parameter estimation of a tungsten chemical vapor deposition system using a reduced order model, paper 193c. In *AIChE Annual Meeting*, Dallas, TX, 1999.
- [20] T. Gougousi, Y. Xu, Jr. J. N. Kidder, G. W. Rubloff, and C. R. Tilford. Process diagnostics and thickness metrology for the chemical vapor deposition of W from  $H_2/WF_6$  using in-situ mass spectrometry. *J. Vac. Sci. Technol. B*, 1999. submitted.
- [21] P. Vandenabeele and W. Renken. The influence of facility conditions on a  $\pm 0.25^\circ\text{C}$  repeatability lamp voltage controlled RTP system. In T. J. Riley et al., editor, *Rapid Thermal and Integrated Processing VI*, volume 470 of *Mat. Res. Soc. Symp. Proc.*, pages 181–186, Pittsburg, PA, 1997. Materials Research Society.
- [22] P. Vandenabeele and W. Renken. Study of repeatability, relative accuracy and lifetime of thermocouple instrumented calibration wafers for RTP. In T. J. Riley et al., editor, *Rapid Thermal and Integrated Processing VI*, volume 470 of *Mat. Res. Soc. Symp. Proc.*, pages 17–22, Pittsburg, PA, 1997. Materials Research Society.
- [23] Computer Boards, Mansfield, MA. *CIO-DAS801 & 802 User's Manual*, revision 1 edition, 1995.

- [24] Computer Boards, Mansfield, MA. *CIO-EXP32/16 Hardware Manual*, revision 4 edition, 1994.
- [25] R. J. Kee, G. Dixon-Lewis, J. Warnatz, M. E. Coltrin, and J. Miller. A FORTRAN computer code package for the evaluation of gas-phase multicomponent transport properties. Technical Report SAND86-8246, Sandia National Laboratories, Albuquerque and Livermore, 1986.
- [26] S. T. Hsu. *Engineering Heat Transfer*. Van Nostrand Co., Princeton, NJ, 1963.
- [27] Properties of silicon. United Kingdom, 1988.
- [28] P. J. Timans. Temperature measurement in rapid thermal processing. *Solid State Technology*, 37(4):63–74, 1997.
- [29] H. K. Moffat and K. F. Jensen. Three-dimensional flow effects in silicon cvd in horizontal reactors. *J. Electrochem. Soc.*, 135(2):459–471, 1988.
- [30] W. L. Holstein and J. L. Fitzjohn. Effect of bouyancy forces and reactor orientation of fluid flow and growth rate uniformity in cold-wall channel CVD reactors. *J. Crystal Growth*, 94:145–158, 1989.
- [31] N. K. Ingle and T. J. Mountziaris. The onset of transverse recirculations during flow of gases in horizontal ducts with differentially heated lower walls. *J. Fluid Mech.*, 277:249–269, 1994.